

This article was downloaded by: [Colorado State University], [Branislav Notaros]

On: 22 April 2014, At: 18:29

Publisher: Taylor & Francis

Informa Ltd Registered in England and Wales Registered Number: 1072954 Registered office: Mortimer House, 37-41 Mortimer Street, London W1T 3JH, UK



Electromagnetics

Publication details, including instructions for authors and subscription information:

<http://www.tandfonline.com/loi/uemg20>

Diakoptic Approach Combining Finite-Element Method and Method of Moments in Analysis of Inhomogeneous Anisotropic Dielectric and Magnetic Scatterers

Ana B. Manić^a, Dragan I. Oléan^b, Milan M. Ilić^{ab} & Branislav M. Notaroš^a

^a Electrical and Computer Engineering Department, Colorado State University, Fort Collins, Colorado, USA

^b School of Electrical Engineering, University of Belgrade, Belgrade, Serbia

Published online: 14 Apr 2014.

To cite this article: Ana B. Manić, Dragan I. Oléan, Milan M. Ilić & Branislav M. Notaroš (2014) Diakoptic Approach Combining Finite-Element Method and Method of Moments in Analysis of Inhomogeneous Anisotropic Dielectric and Magnetic Scatterers, *Electromagnetics*, 34:3-4, 222-238, DOI: [10.1080/02726343.2014.877755](https://doi.org/10.1080/02726343.2014.877755)

To link to this article: <http://dx.doi.org/10.1080/02726343.2014.877755>

PLEASE SCROLL DOWN FOR ARTICLE

Taylor & Francis makes every effort to ensure the accuracy of all the information (the "Content") contained in the publications on our platform. However, Taylor & Francis, our agents, and our licensors make no representations or warranties whatsoever as to the accuracy, completeness, or suitability for any purpose of the Content. Any opinions and views expressed in this publication are the opinions and views of the authors, and are not the views of or endorsed by Taylor & Francis. The accuracy of the Content should not be relied upon and should be independently verified with primary sources of information. Taylor and Francis shall not be liable for any losses, actions, claims, proceedings, demands, costs, expenses, damages, and other liabilities whatsoever or howsoever caused arising directly or indirectly in connection with, in relation to or arising out of the use of the Content.

This article may be used for research, teaching, and private study purposes. Any substantial or systematic reproduction, redistribution, reselling, loan, sub-licensing, systematic supply, or distribution in any form to anyone is expressly forbidden. Terms &

Conditions of access and use can be found at <http://www.tandfonline.com/page/terms-and-conditions>

Diakoptic Approach Combining Finite-Element Method and Method of Moments in Analysis of Inhomogeneous Anisotropic Dielectric and Magnetic Scatterers

ANA B. MANIĆ,¹ DRAGAN I. OLCAN,² MILAN M. ILIĆ,^{1,2}
and BRANISLAV M. NOTAROS¹

¹Electrical and Computer Engineering Department, Colorado State University,
Fort Collins, Colorado, USA

²School of Electrical Engineering, University of Belgrade, Belgrade, Serbia

Abstract *A new diakoptic method combining the finite-element method and the method of moments is proposed for analysis of inhomogeneous anisotropic dielectric and magnetic scatterers. The method splits the original electromagnetic system into a number of closed-region finite-element method subsystems containing material complexities and an open-region method of moments subsystem, which are analyzed independently. The solution to the original problem is obtained from linear relations between coefficients in expansions of equivalent electric and magnetic surface currents on diakoptic boundary surfaces. Diakoptic electric sources and the magnetic field in finite-element method subsystems are connected using dual sets of higher-order hierarchical basis functions.*

Keywords diakoptic analysis, domain decomposition, finite-element method, higher-order modeling, numerical techniques, surface equivalence principle, scattering, inhomogeneous anisotropic materials

1. Introduction

The finite-element method (FEM) is, by its inherent features, especially suitable for modeling and analysis of structures that contain inhomogeneous, complex electromagnetic materials, and geometrical irregularities. The FEM is well established as a method of choice for such applications, with the analysis of open-region scattering structures being performed, truncating the FEM domain by a hybridization with the method of moments (MoM) or by some sort of a boundary condition. On the other hand, one possible general strategy aimed at extending the practical applicability of the FEM over its inherent numerical limit and considerably enhancing its efficiency in real-world simulations is the diakoptic approach (Olčan et al., 2006, 2007, 2008a, 2008b, 2010; Manić et al., 2012b,

Received 14 August 2013; accepted 28 October 2013.

Address correspondence to Branislav M. Notaros, Department of Electrical and Computer Engineering, Colorado State University, 1373 Campus Delivery, Fort Collins, CO 80523-1373. E-mail: notaros@colostate.edu

Color versions of one or more of the figures in the article can be found online at www.tandfonline.com/uemg.

2013), according to which the solution of a large and complex electromagnetic system is found as a linear combination of solutions of diakoptic subsystems, using explicit linear relations between coefficients in expansions of equivalent electric and magnetic surface currents on boundary surfaces of subsystems.

The diakoptic analysis of electromagnetic systems is formally similar to the diakoptic approach in circuit theory (Kron, 1963). However, the present diakoptic analysis is based on the surface equivalence principle and operates with coefficients in expansions of surface electric and magnetic currents and volume electromagnetic fields. The diakoptic analysis also belongs to the class of domain decomposition methods (Lee et al., 2005; Li & Jin, 2007; Zhao et al., 2008; Ilić & Notaroš, 2009). However, diakoptics explicitly takes into account linear relations between coefficients of the equivalent surface current expansions, with each electromagnetic subsystem being represented by linear relations written in the form of matrices. In addition, the diakoptic approach uses a direct solution of the diakoptic linear system of equations.

This article presents a new FEM-MoM-diakoptic method for analysis of inhomogeneous anisotropic dielectric and magnetic scatterers in the frequency domain as a continuation of the work in Manić et al. (2012b, 2013) and Olćan et al. (2006, 2007, 2008a, 2008b, 2010). The method splits the original electromagnetic system into a number of closed-region subsystems containing material complexities, analyzed by an FEM technique (FEM diakoptic subsystems), and an open-region subsystem enclosing the FEM subsystems, analyzed by an MoM technique (MoM diakoptic subsystem). Each of the subsystems is analyzed completely independently, applying FEM or MoM solvers to obtain linear relations between coefficients in the expansions of equivalent electric and magnetic surface currents on the boundary surface of each subsystem (diakoptic surfaces). In the final system of equations, the only unknowns are the expansion coefficients on diakoptic surfaces.

The method implements Lagrange-type generalized curved parametric hexahedral finite elements of arbitrary geometrical-mapping orders, filled with inhomogeneous anisotropic materials with continuous spatial variations of complex relative permittivity and permeability tensors described by Lagrange interpolation polynomials of arbitrary material-representation orders. Curl-conforming hierarchical polynomial vector basis functions of arbitrary field-expansion orders are used for the approximation of the electric field vector within the finite elements, while divergence-conforming higher-order vector bases on generalized curved parametric quadrilaterals are implemented for diakoptic surfaces. Furthermore, the connection between the diakoptic electric sources and the magnetic field in the FEM subsystems is enforced using dual sets of higher-order basis functions explicitly satisfying the natural relation between curl-conforming and divergence-conforming quantities when closing the FEM domain by a boundary surface with fictitious equivalent surface currents. Finally, this diakoptic method inherently allows touching of the subsystems; i.e., the subsystems can share a common diakoptic boundary—without requirements for introduction of additional basis functions. Note that, theoretically, the diakoptic surfaces can be anywhere: away from the scatterers, at the boundary of a scatterer, or even crossing the volume of a scatterer.

The rest of this article is organized as follows. Section 2 presents the theory of the FEM-MoM-diakoptic method for analysis of inhomogeneous anisotropic dielectric and magnetic scatterers, starting with the surface equivalence principle, and deriving linear relations between diakoptic coefficients and representing electromagnetic subsystems by diakoptic matrices. It also presents the implementation of the method based on a magnetic-field FEM diakoptic formulation and double-higher-order numerical discretization. In

Section 3, the proposed diakoptic method is validated in several characteristic scattering examples.

2. FEM-MoM-Diakoptic Method for Inhomogeneous Anisotropic Scatterers

2.1. Theory of FEM-MoM-Diakoptics for Scattering Analysis

The diakoptic method is based on the surface equivalence principle (Kolundžija & Djordjević, 2002; Harrington, 2001). For instance, consider an arbitrary closed surface S , as shown in Figure 1(a), which divides the original electromagnetic system into two regions, with sources of electromagnetic fields (e.g., lumped generators or incident fields in the system) assumed to exist in both regions. Employing the surface equivalence principle, equivalent sources are placed at each side of the boundary S (in each of the regions) and are chosen so that the electric and magnetic fields generated by the sources inside each individual region remain the same as in the original system, while the fields in the other region are annulled, as illustrated in Figures 1(b) and 1(c). For the inner region (reg 1), the densities of equivalent electric and magnetic surface currents are given by $\mathbf{J}_e^{\text{reg1}} = \mathbf{n} \times \mathbf{H}_{1S}$ and $\mathbf{M}_e^{\text{reg1}} = -\mathbf{n} \times \mathbf{E}_{1S}$, where \mathbf{n} denotes the inward looking unit normal on S , and \mathbf{E}_{1S} and \mathbf{H}_{1S} stand for the electric and magnetic field vectors, respectively, on the inner side of S in the original system in Figure 1(a). The equivalent sources for the outer region (reg 2) are obtained in an analogous fashion. Applying the tangential continuity conditions for the fields in the original system, the following relations between equivalent sources for the two regions are obtained:

$$\mathbf{J}_e^{\text{reg1}} = -\mathbf{J}_e^{\text{reg2}} \quad \text{and} \quad \mathbf{M}_e^{\text{reg1}} = -\mathbf{M}_e^{\text{reg2}}, \quad (1)$$

which will later be used explicitly to connect unknown variables in the diakoptic method.

Next, the example depicted in Figure 2 is used to describe the implementation of the diakoptic analysis combining FEM and MoM solvers. The diakoptic approach starts with subdividing the original electromagnetic system into a number of arbitrary non-overlapping subsystems, as shown in Figure 2(a), where the so-called diakoptic boundary is the surface enclosing different subsystems and, in general, containing a number of disconnected closed surfaces. In the present method, an FEM technique is used for the

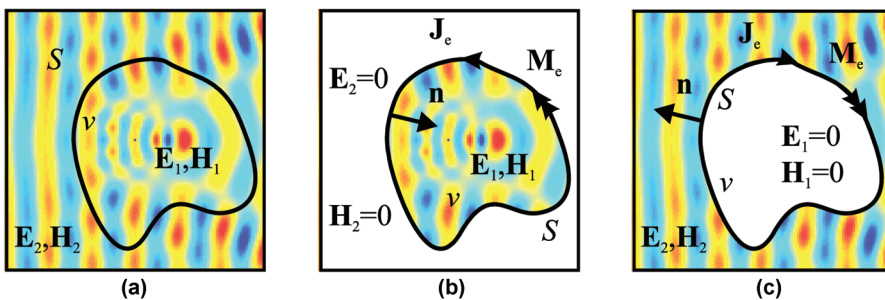


Figure 1. Illustration of the surface equivalence principle as the theoretical foundation of the FEM-MoM-diakoptic method: (a) original electromagnetic system, (b) equivalent problem for interior region, and (c) equivalent problem for exterior region.

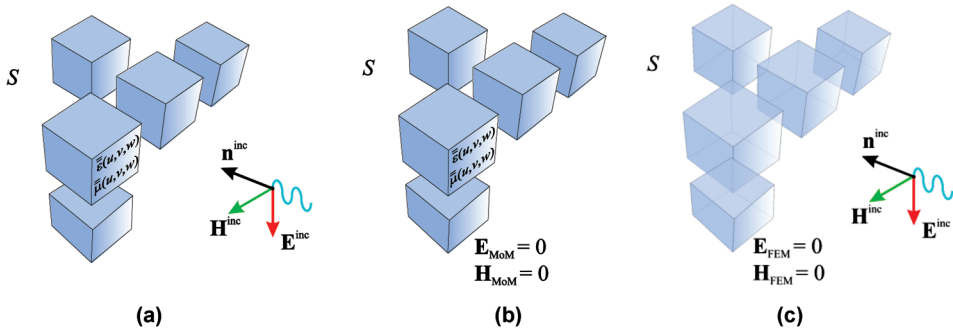


Figure 2. Application of FEM-MoM-diakoptic technique for scattering analysis: (a) original electromagnetic system split into $N_{FEM} + 1$ parts (subsystems), (b) N_{FEM} closed-region subsystems containing material complexities analyzed by FEM technique (FEM diakoptic subsystems), and (c) an open-region subsystem analyzed by MoM technique (MoM diakoptic subsystem).

analysis of each of the closed-region subsystems (N_{FEM} FEM subsystems), as indicated in Figure 2(b), while the open-region subsystem, shown in Figure 2(c), is analyzed invoking an MoM technique (MoM subsystem). Second, the diakoptic boundary is used as an interface between the FEM and MoM domains (subsystems) employing the surface equivalence principle (Figure 1) and allowing each of the subsystems to be independently analyzed and then connected back together through relations in Eq. (1). Consequently, when implementing the diakoptic approach using FEM and MoM solvers, the unknowns, in general, are (i) distributions of electric and magnetic fields of intensities \mathbf{E} and \mathbf{H} in the FEM regions and (ii) distributions of equivalent surface electric and magnetic currents of densities \mathbf{J}_e and \mathbf{M}_e at the diakoptic boundary.

Let the total number of unknown coefficients for the approximation of \mathbf{E} and \mathbf{H} , placed in column-matrices $[\mathbf{e}]$ and $[\mathbf{h}]$, respectively, for all FEM subsystems be $N_{tot}^{FEM} = N_{tot}^e + N_{tot}^h$, where $N_{tot}^e = \sum_{i=1}^{N_{FEM}} N_i^e$ and $N_{tot}^h = \sum_{i=1}^{N_{FEM}} N_i^h$ are the total numbers of coefficients in $[\mathbf{e}]$ and $[\mathbf{h}]$, and N_i^e and N_i^h are the respective numbers of coefficients for the i th FEM subsystem. In addition, there are $2D$ unknowns for the approximation of \mathbf{J}_e and \mathbf{M}_e at the diakoptic boundary (the union of N_{FEM} disconnected boundary surfaces in Figure 2(b)), namely, D coefficients for \mathbf{J}_e in the column-matrix $[\mathbf{j}_e]$ and the same number of coefficients for \mathbf{M}_e in $[\mathbf{m}_e]$, where $D = \sum_{i=1}^{N_{FEM}} D_i$, with D_i being the number of diakoptic coefficients associated with the i th FEM subsystem ($i = 1, 2, \dots, N_{FEM}$). It is essential that the column-matrices $[\mathbf{j}_e]$ and $[\mathbf{m}_e]$ are of the same dimensions.

Based on the linearity of the electromagnetic system in Figure 2(a), the objective of the diakoptic analysis of each of the subsystems in Figures 2(b) and 2(c) is to define linear relations between electric and magnetic diakoptic sources belonging to the diakoptic boundary of the subsystem in the following form:

$$[\mathbf{j}_{ek}] = [\mathbf{Y}_k][\mathbf{m}_{ek}] + [\mathbf{j}_{ek}]_0, \quad k = 1, 2, \quad (2)$$

where $k = 1$ denotes the inner side (FEM side) of the union of all disconnected diakoptic subdomains, $k = 2$ denotes the outer side (MoM side) of the same union, $[\mathbf{Y}_k]$ is the $D \times D$ diakoptic matrix of the subsystem, $[\mathbf{j}_{ek}]_0$ is the $D \times 1$ column matrix containing coefficients of \mathbf{J}_e that represent the excitation in the subsystem. To numerically calculate

the matrix $[\mathbf{Y}_k]$, it is assumed that all excitations in the subsystem are turned off and that the subsystem is excited with one, the j th, unit-valued coefficient in $[\mathbf{m}_{ek}]$, while all other coefficients in $[\mathbf{m}_{ek}]$ are equal to zero. By using the FEM solver, coefficients of \mathbf{E} , \mathbf{H} , and \mathbf{J}_e are calculated in the FEM subsystems, with the obtained coefficients of \mathbf{J}_e representing, numerically, the j th column of the matrix $[\mathbf{Y}_k]$, and similarly for the MoM subsystems. While MoM matrices are dense, FEM matrices are sparse and are stored and computed as such.

In the same analysis, the linear relations between coefficients in $[\mathbf{m}_{e1}]$ and those in $[\mathbf{e}]$ and $[\mathbf{h}]$ are obtained. These relations can be written as

$$\begin{bmatrix} \mathbf{e} \\ \mathbf{h} \end{bmatrix} = [\mathbf{C}][\mathbf{m}_{e1}] + \begin{bmatrix} \mathbf{e} \\ \mathbf{h} \end{bmatrix}_0, \quad (3)$$

with $[\mathbf{C}]$ being of dimensions $N_{\text{tot}}^{\text{FEM}} \times D$. The matrix $[\mathbf{C}]$ is evaluated during the calculation of matrices $[\mathbf{Y}_1]$ in the same way, column by column, exciting the respective subsystem by a single coefficient in $[\mathbf{m}_{e1}]$ at the time, with the computed coefficients of \mathbf{E} and \mathbf{H} thus filling the respective column of the matrix $[\mathbf{C}]$ and stored to be used for subsequent calculation of the final solution.

The excitations $[\mathbf{j}_{ek}]_0$ and $[\mathbf{h}_e^e]_0$ in Eqs. (2) and (3) are found as the responses of a given subsystem stipulating that all coefficients in $[\mathbf{m}_{ek}]$ are set to zero, while the original excitation is turned on. By the standard FEM and MoM analysis, the coefficients of \mathbf{J}_e , \mathbf{E} , and \mathbf{H} are calculated, which constitute, in the numerical sense, the respective column-matrices $[\mathbf{j}_{ek}]_0$ and $[\mathbf{h}_e^e]_0$. The relations in Eqs. (2) and (3) will be discussed in the following sections with specifics given for both FEM and MoM solvers.

To obtain the solution of the original electromagnetic problem (Figure 2(a)), using matrices that represent different subsystems in Eqs. (2) and (3), the diakoptic coefficients of \mathbf{J}_e and \mathbf{M}_e are related on the diakoptic boundary between FEM and MoM subsystems as follows:

$$-[\mathbf{j}_{e1}] = [\mathbf{j}_{e2}] = [\mathbf{j}_e], \quad -[\mathbf{m}_{e1}] = [\mathbf{m}_{e2}] = [\mathbf{m}_e], \quad (4)$$

utilizing the facts that the equivalent sources in Eq. (1) have opposite signs and that the directions of vectors \mathbf{n} in Figures 1(b) and 1(c) are opposite. Note that the mutual relations connecting the diakoptic coefficients obtained for the interior side of the diakoptic surface for any subsystem must also be satisfied on the surface outside that subsystem. This property is further used when combining Eqs. (2) and (4) to arrive to the following diakoptic matrix system of equations:

$$([\mathbf{Y}_1] - [\mathbf{Y}_2])[\mathbf{m}_e] = -[\mathbf{j}_{e1}]_0 + [\mathbf{j}_{e2}]_0, \quad (5)$$

whose solution is $[\mathbf{m}_e]$. This system of equations is solved with a direct solver (i.e., the system is factorized using lower-upper (LU) decomposition, carrying out partial pivoting with row interchanges, and then forward and backward substitutions are performed), since it is dense in the general case. The diakoptic coefficients in $[\mathbf{j}_{ek}]$ ($k = 1, 2$) are then computed from $[\mathbf{m}_e]$ using Eq. (2), and the coefficients in $[\mathbf{e}]$ and $[\mathbf{h}]$, for subsystems in Figures 2(b) and 2(c), are obtained from Eq. (3). Once these latter coefficients are obtained, the electromagnetic field at any point in space can be calculated, as well as any other quantity of interest for the original electromagnetic structure (in Figure 2(a)).

2.2. Double-Higher-Order Magnetic-Field FEM Diakoptic Implementation

The diakoptic method described in the previous sections is now applied in conjunction with double-higher-order FEM and MoM solvers based on higher-order geometrical modeling and higher-order field/current modeling. In specific, the building block for volumetric modeling in FEM subsystems (Figure 2(b)) is a Lagrange-type interpolation generalized hexahedron of arbitrary geometrical orders K_u , K_v , and K_w ($K_u, K_v, K_w \geq 1$), shown in Figure 3(a) and analytically described as (Ilić & Notaroš, 2003)

$$\mathbf{r}(u, v, w) = \sum_{i=0}^{K_u} \sum_{j=0}^{K_v} \sum_{k=0}^{K_w} \mathbf{r}_{ijk} L_i^{K_u}(u) L_j^{K_v}(v) L_k^{K_w}(w),$$

$$L_i^{K_u}(u) = \prod_{\substack{l=0 \\ l \neq i}}^{K_u} \frac{u - u_l}{u_l - u_i},$$

$$-1 \leq u, v, w \leq 1,$$

where $\mathbf{r}_{ijk} = \mathbf{r}(u_i, v_j, w_k)$ are position vectors of interpolation nodes, and $L_i^{K_u}(u)$ represents Lagrange interpolation polynomials in the u coordinate, with u_i being defined as $u_i = (2i - K_u)/K_u$ ($i = 0, 1, \dots, K_u$) and similarly for $L_j^{K_v}(v)$ and $L_k^{K_w}(w)$.

The same polynomials in Eq. (6) are used to describe the continuous spatial variations of both the complex permittivity and permeability tensors, $\bar{\epsilon}(u, v, w)$ and $\bar{\mu}(u, v, w)$, of an inhomogeneous anisotropic material filling the generalized hexahedral element in Figure 3(a), as proposed in Manić et al. (2012a). In specific, the xx -component of $\bar{\epsilon}$ is

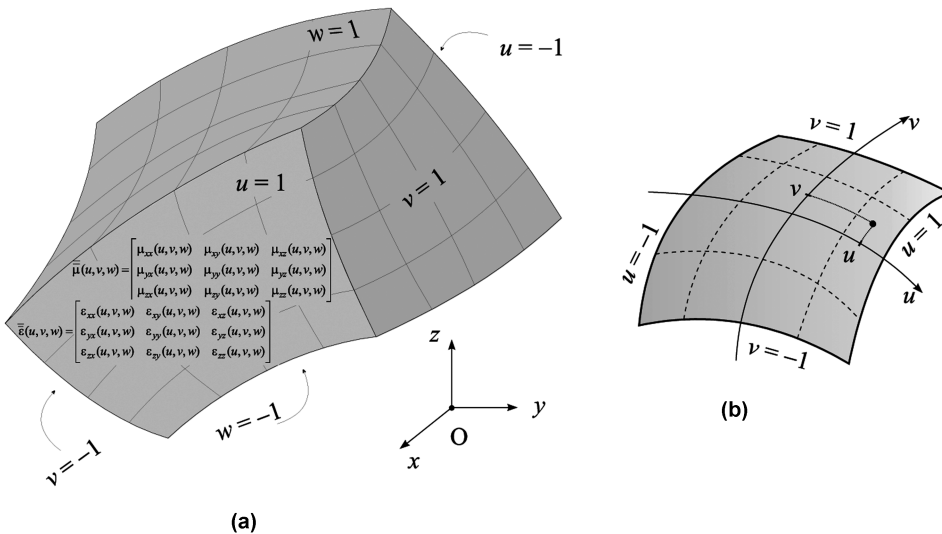


Figure 3. Lagrange-type curved parametric elements for higher-order FEM-MoM-diakoptic analysis (Figure 2) of inhomogeneous anisotropic dielectric and magnetic scatterers: (a) generalized FEM hexahedron defined by Eq. (6) and (b) generalized MoM quadrilateral patch.

incorporated in the FEM model as

$$\varepsilon_{xx}(u, v, w) = \sum_{m=0}^{M_u} \sum_{n=0}^{M_v} \sum_{p=0}^{M_w} \varepsilon_{xx}^{mnp} L_m^{M_u}(u) L_n^{M_v}(v) L_p^{M_w}(w), \quad (7)$$

where M_u , M_v , and M_w ($M_u, M_v, M_w \geq 1$) are arbitrary material-representation polynomial orders (independent from K_u , K_v , and K_w); $\varepsilon_{xx}^{mnp} = \varepsilon_{xx}(\mathbf{r}_{mnp})$ denotes the respective permittivity values at interpolation nodes \mathbf{r}_{mnp} corresponding to orders M_u , M_v , and M_w , and similarly for all remaining components of $\bar{\varepsilon}$ and for all components of $\bar{\mu}$.

The diakoptic surface enclosing each of the FEM domains is modeled using Lagrange-type generalized curved parametric quadrilaterals in Figure 3(b) (Djordjević & Notaroš, 2004), which are surface two-dimensional (2-D) versions of the hexahedron in Figure 3(a) and are conformal with the sides of hexahedra belonging to the diakoptic surface (Ilić et al., 2009).

This work utilizes the H -field FEM formulation (except in the last example, where the E -field FEM formulation is used) and expands the magnetic field by means of curl-conforming hierarchical polynomial vector basis functions of arbitrary field-expansion orders N_u , N_v , and N_w ($N_u, N_v, N_w \geq 1$) introduced in Ilić and Notaroš (2003). Furthermore, in the field expansion, basis functions that possess tangential components at the boundary (marked by “boundary”) are distinguished from those that do not (“interior”), as described in Jin and Riley (2008):

$$\mathbf{H} = \sum_{i=1}^{N_{\text{tot}}^h} \mathbf{h}_i \mathbf{f}_i = \sum_{i=1}^{N_{\text{INTERIOR}}} \mathbf{h}_{iI} \mathbf{f}_{iI} + \sum_{i=1}^{N_{\text{BOUNDARY}}} \mathbf{h}_{iB} \mathbf{f}_{iB} \quad (8)$$

Boundary volume basis functions are further used to generate divergence-conforming surface basis functions as $\mathbf{n} \times \mathbf{f}_{Bi}|_S$ for expanding the diakoptic surface currents in the following form (Manić et al., 2013):

$$\mathbf{J}_e = \mathbf{n} \times \mathbf{H}|_S = \sum_{i=1}^{N_{\text{BOUNDARY}}} \mathbf{j}_{ei} (\mathbf{n} \times \mathbf{f}_{Bi}) \Big|_S, \quad (9)$$

$$\mathbf{M}_e = -\mathbf{n} \times \mathbf{E}|_S = \sum_{i=1}^{N_{\text{BOUNDARY}}} \mathbf{m}_{ei} (\mathbf{n} \times \mathbf{f}_{Bi}) \Big|_S, \quad (10)$$

where \mathbf{n} is adopted to be the outward looking unit normal to the enclosed diakoptic surface S .

To numerically establish the matrix relationships in Eq. (2), the FEM solver discretizes a Galerkin-type weak form of the curl-curl magnetic-field vector wave equation

$$\int_V (\nabla \times \mathbf{f}_i) \cdot (\bar{\varepsilon}_r^{-1} \nabla \times \mathbf{H}) dV - k_0^2 \int_V \mathbf{f}_i \cdot (\bar{\mu}_r \mathbf{H}) dV = jk_0 \oint_S \mathbf{f}_i \cdot (\mathbf{n} \times \mathbf{E}) dS, \quad (11)$$

with $k_0 = \omega \sqrt{\varepsilon_0 \mu_0}$ being the free-space wave number (ω is the angular frequency of the time-harmonic excitation in the system). This discretization leads to a matrix equation with the unknowns coefficients being only those describing boundary variables,

$$[F_{\text{BB}} - F_{\text{BI}} (F_{\text{II}}^{-1} F_{\text{IB}})] [\mathbf{h}_{\text{B}}] = -jk_0 [(\mathbf{f}_{\text{B}}, \mathbf{n} \times \mathbf{f}_{\text{B}})] [\mathbf{m}_{\text{e}}], \quad (12)$$

and in which the connection in Eq. (10) is employed on the right-hand side of the equation such that magnetic diakoptic sources can numerically be considered as excitation of the system. In Eq. (12), F_{BB} , F_{BI} , F_{IB} , and F_{II} are the submatrices of a well-known FEM matrix (Ilić & Notaroš, 2003), with F_{IB} , for instance, standing for the submatrix corresponding to testing functions belonging to a set of the interior FEM functions and basis functions being the boundary functions, and the operator $\langle \mathbf{a}, \mathbf{b} \rangle$ is a standard surface integral of a dot product of vector variables \mathbf{a} and \mathbf{b} . Note that while the matrix $[\langle \mathbf{f}_B, \mathbf{n} \times \mathbf{f}_B \rangle]$ in Eq. (12) is ill-conditioned, this does not deteriorate the overall accuracy of the method, as shown in examples presented in this article (and evaluated in other cases that are not shown).

Next, boundary coefficients in the expansion of the magnetic field are equated to the appropriate electric-current coefficients using Eq. (9) so that a diakoptic linear relation in Eq. (2) can be established by inverting the system matrix in Eq. (12). Denoting the local diakoptic matrix of the i th FEM subsystem in Figure 2(b) by $[\mathbf{Y}_1^i]$ and the corresponding source column-matrices by $[\mathbf{m}_e^i]$ and $[\mathbf{j}_e^i]$ gives

$$\begin{aligned} [\mathbf{Y}_1^i] [\mathbf{m}_e^i] &= [\mathbf{j}_e^i], \\ [\mathbf{Y}_1^i] &= -jk_0 [F_{BB} - F_{BI} (F_{II}^{-1} F_{IB})]^{-1} [\langle \mathbf{f}_B, \mathbf{n} \times \mathbf{f}_B \rangle], \\ i &= 1, 2, \dots, N_{\text{FEM}}, \end{aligned} \quad (13)$$

and the global diakoptic matrix $[\mathbf{Y}_1]$ given in Eq. (5) is then assembled using the local matrices as follows:

$$[\mathbf{Y}_1] = \begin{matrix} & D_1 & D_2 & \cdots & D_{N_{\text{FEM}}} \\ & \leftrightarrow & \leftrightarrow & & \leftrightarrow \\ D_1 \downarrow & \mathbf{Y}_1^1 & & & \\ D_2 \downarrow & & \mathbf{Y}_1^2 & & \\ \vdots & & & \ddots & \\ D_{N_{\text{FEM}}} \downarrow & & & & \mathbf{Y}_1^{N_{\text{FEM}}} \end{matrix}. \quad (14)$$

Once the diakoptic excitations $[\mathbf{m}_e]$ are found from Eq. (5), the magnetic field inside each of the FEM domains can be calculated based on Eq. (3) using $[\mathbf{C}]$, which, in turn, can easily be obtained from Eq. (11) in terms of appropriate local matrices in the same fashion as in Eq. (14).

In cases where the original electromagnetic system (Figure 2(a)) is subdivided into a number of touching FEM subsystems, the adjacent subsystems touch each other through parts of the diakoptic surface, which is meshed in a way that a generalized quadrilateral patch belonging to one side of the common area has its match on the opposite side; i.e., the meshes on opposite sides of the diakoptic surface are conformal. Even though spatial positions of touching quadrilaterals are the same, independent subsystems are pre-processed separately. In this setup, the touching quadrilaterals need to have opposite orientations; that is, the directions of normal vectors \mathbf{n} should be opposite to one another, which is ensured by a simple adjustment of the two local parametric coordinate systems for the two coinciding patches. Next, touching subsystems are assumed to be immersed in the air-filled open-region subsystem; hence, an infinitesimally thin layer of air is considered to exist between the touching quadrilaterals. Consequently, touching FEM domains influence each other through an MoM domain, where a numerical solver is applied to

a structure consisting of touching and other surfaces. The only issue with applying the MoM solver relates to the calculation of singular and hyper-singular Galerkin impedance matrix elements (Djordjević & Notaroš, 2004) due to the mutual contributions of surface currents belonging to two touching surfaces. Since touching surfaces (faces of the adjacent diakoptic domains), although belonging to two distinct diakoptic domains, actually share a unique surface in space, the corresponding Galerkin impedances are computed by applying a self-integration procedure, with testing and basis functions belonging to the two distinct surfaces coinciding in space. Namely, the singularity extraction method for calculation of singular and hyper-singular MoM operators (Notaroš, 2008; Djordjević & Notaroš, 2004; Notaroš & Popović, 1997) is utilized. Note also that in the case of touching domains, matrix $[\mathbf{Y}_2]$ is not diagonal-dominant, and it influences the final matrix obtained by the diakoptic method.

Note, finally, that any other FEM and/or MoM numerical discretization is possible within the framework of the diakoptics, including low-order elements and bases.

3. Numerical Results

A special parallel version of the FEM-MoM-diakoptic solver based on the message passing interface (MPI) basic linear algebra communication subprograms (BLACS) is developed and run on a CrayXT6m platform (Cray Inc., 2011). The Cray supercomputer used for simulations contains 52 compute nodes, with a total of 104 AMD Magny Cours 64-bit 1.9-GHz processors (two per node), where each processor has 12 cores. Thirty-two GB of RAM is available on each node, while the interconnection between the nodes is SeaStar2+ with 2D torus topology.

3.1. 2-D Array of Dielectrically Coated Perfect Electric Conductor (PEC) Spherical Scatterers

As the first example of the application and validation of the new diakoptic method, consider a 2-D array of 4×4 dielectrically coated spherical PEC scatterers, depicted in Figure 4. For each scatterer, the PEC sphere radius is $r = 100$ mm, and the thickness

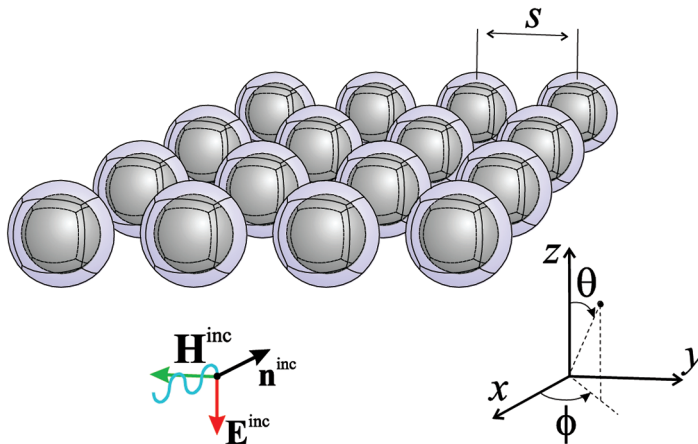


Figure 4. 2-D array of dielectrically coated spherical PEC scatterers.

and relative permittivity of the coating are $d = 35$ mm and $\varepsilon_r = 4$, respectively, while the center-to-center distances between adjacent scatterers are $s = 400$ mm. The original system is divided into 17 diakoptic subsystems, with 16 FEM subsystems modeling individual spherical scatterers and 1 open-region MoM subsystem. The geometrical model of each spherical scatterer is comprised of six FEM curvilinear hexahedra of the second geometrical orders ($K_u = K_v = K_w = 2$) modeling the dielectric coating, with PEC boundary conditions on the inner surfaces and six curvilinear quadrilateral patches on the outer surfaces, coinciding with the adopted diakoptic boundary. The adopted field approximation orders in all FEM hexahedra are $N_w = 2$ in the radial direction and $N_u = N_v = 4$ in other two (transversal) directions, and these latter orders are used for current expansions on the MoM patches (on the diakoptic boundaries) as well. This results in a total of $D = 3,072$ diakoptic unknowns.

Figure 5 presents the normalized bistatic radar cross-section (RCS), σ_{3D}/λ_0^2 (λ_0 henceforth being the free-space wavelength), of the array at a frequency $f = 0.5$ GHz as a function of the scattered angle in two characteristic plane cuts. The excitation wave is incident from the direction defined by $\theta_{inc} = 90^\circ$ and $\phi_{inc} = 0$, where θ and ϕ are angular coordinates in the spherical coordinate system shown in Figure 4. The same (θ, ϕ) notation will be used in all examples in this section. Excellent agreement of diakoptic results is observed with the solution obtained by WIPL-D (pure-MoM commercial software; WIPL-D d.o.o., 2013), which serves as a reference. The total number of unknowns used for modeling in WIPL-D is 9,216. The approximately three-times reduction in the number of the diakoptic unknowns, when compared with the commercial higher order MoM software, comes from the implemented geometrically higher-order modeling and diakoptic compression. Note also that the analysis of this problem using a low-order variant of the proposed diakoptic method, with first-order (rooftop) basis functions on patches that are not larger than $\lambda/10$ in each dimension (with λ being the wavelength in the dielectric medium), would require $D = 19,200$ diakoptic unknowns and about 244 times longer time to solve the matrix system of equations and about 39 times greater RAM for the simulation than the presented higher-order diakoptic solution.

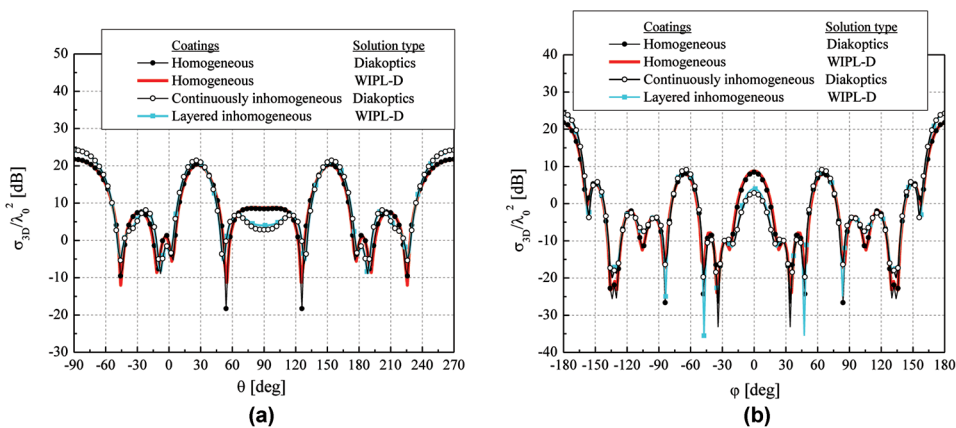


Figure 5. Normalized bistatic RCS of the array of scatterers in Figure 4 for homogeneous and continuously inhomogeneous dielectric coatings, respectively, computed by the FEM-MoM-diakoptic method and by the pure-MoM commercial software WIPL-D: (a) $\phi = 0^\circ$ cut and (b) $\theta = 90^\circ$ cut.

In addition, Figure 5 gives the RCS results for the same geometry and frequency but with the dielectric coating being made from a continuously inhomogeneous dielectric material whose relative permittivity undergoes a linear radial variation from $\epsilon_r = 4$ at the PEC boundary to $\epsilon_r = 10$ at the outer surface of the scatterer. The higher-order geometrical and numerical model is the same as in the previous case but with $M = 1$ in Eq. (7) for the local radial direction to model the dielectric inhomogeneity. The solution using the continuously inhomogeneous FEM-MoM-diaoptical model is compared with a WIPL-D solution for a three-layer piecewise homogeneous approximate model of the dielectric coating (with equivalent permittivities calculated as the mean value of the inhomogeneous profile for each of the equally thick layers), which takes 51,712 unknowns, and a good agreement of the two sets of results is observed.

The total computation time for the FEM-MoM-diaoptical analysis of scatterers with both homogeneous and continuously inhomogeneous dielectrics (in Figure 5) is 2 min 27 sec, and the RAM used for the storage of the diaoptical matrices is 288 MB; running the parallel code on a 2×2 process grid, all processes are on a single compute node.

3.2. Dielectric Scatterer Modeled by Multiple Touching FEM Domains

The next example considers a dielectric ($\epsilon_r = 2.25$) brick-shaped scatterer, shown in Figure 6, illuminated by a uniform plane wave incident from the direction defined by $\theta_{\text{inc}} = 90^\circ$ and $\phi_{\text{inc}} = 0$, with electric and magnetic field vectors given by $\mathbf{E}^{\text{inc}} = -1\mathbf{i}_z$ V/m and $\mathbf{H}^{\text{inc}} = -\eta_0^{-1}\mathbf{i}_y$ A/m at the global coordinate origin, where $\eta_0 = \sqrt{\mu_0/\epsilon_0}$ stands for the free-space intrinsic impedance. The operating frequency is $f = 250$ MHz. The brick is modeled by four adjacent cubical FEM elements, each with edge length $a = 1$ m and enclosed by the diaoptical surface with air as the outer medium. All elements in the model are of the first geometrical order ($K_u = K_v = K_w = 1$), whereas the orders of the field expansions (in all FEM elements in all directions) and current expansions (on all square MoM patches surrounding each of the FEM subdomains) are all the same and equal to 5. The total number of unknowns in the final system of equations is $D = 1,200$, while the total number of unknown coefficients used for magnetic field expansion is $N_{\text{tot}}^h = 2,160$.

Shown in Figure 7(a) is the computed real part of H_y in the FEM domains in the vertical plane defined by $x = 0$ placed in the middle of the scatterer. For comparison,

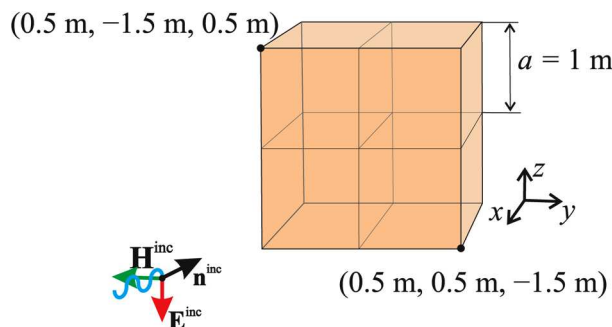


Figure 6. Brick-shaped dielectric scatterer modeled by four touching cubical FEM diaoptical sub-systems.

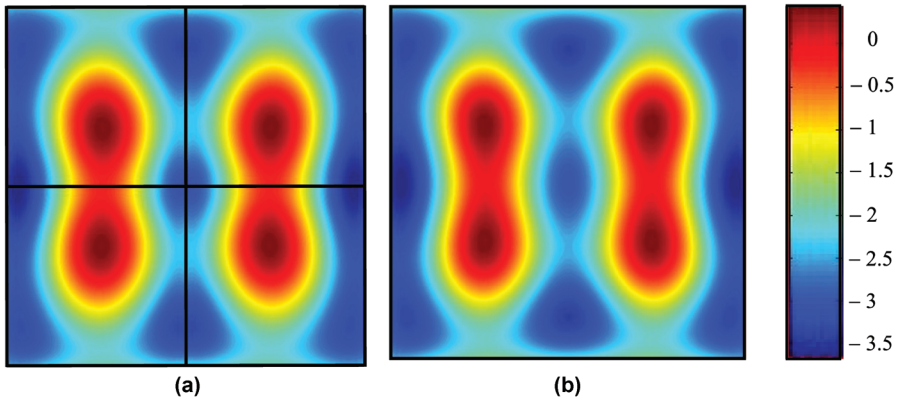


Figure 7. Real part of the internal magnetic field component H_y in the vertical plane ($x = 0$) in the middle of the scatterer in Figure 6 obtained by: (a) FEM-MoM-diakoptic method and (b) WIPL-D (color bar units are in mA/m).

the same solution obtained by WIPL-D is shown in Figure 7(b) as a reference. It can be concluded from the figure that the agreement of the diakoptic results with the reference results is very good. Running the code in a single process, the FEM-MoM-diakoptic solution takes 56 sec of simulation time and uses 43.9 MB of RAM to store the diakoptic matrices.

3.3. 3-D Array of Cubical Dielectric Scatterers

Next, consider a three-dimensional (3-D) array of cubical dielectric scatterers, shown in Figure 8. The cube edges and side-to-side distances between neighboring cubes amount to $a = s = 1\lambda_0$, and the relative permittivity of the dielectric is $\epsilon_r = 2.25$. The structure is modeled by 513 diakoptic subsystems (512 FEM domains and 1 open-region MoM domain). The volume and surface elements in the model are of the first geometrical orders, $K_u = K_v = K_w = 1$, while the field and current expansion orders are all the same and equal to 3. The size of the system of diakoptic equations is $D = 55,296$.

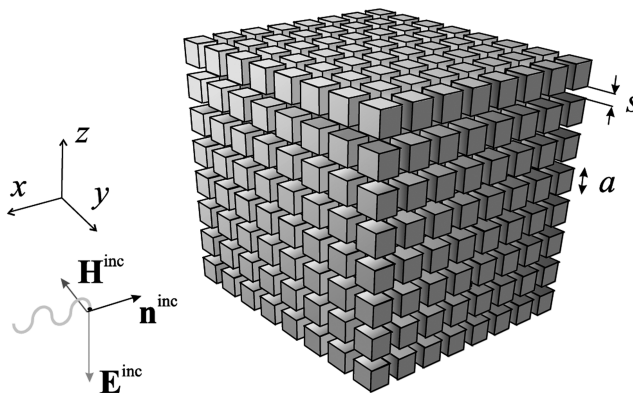


Figure 8. 3-D array of cubical dielectric scatterers.

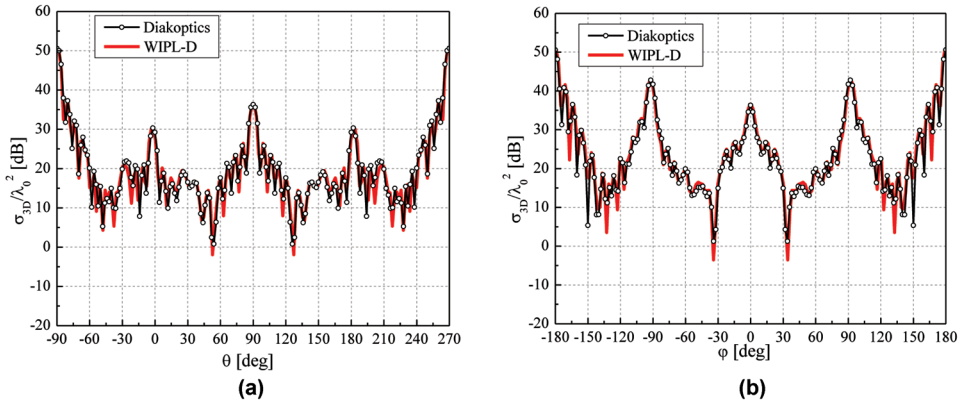


Figure 9. Normalized bistatic RCS of array of scatterers in Figure 8 obtained by FEM-MoM-diakoptic method and by WIPL-D: (a) $\phi = 0^\circ$ cut and (b) $\theta = 90^\circ$ cut.

Figure 9 displays two characteristic normalized bistatic RCS plane cuts for uniform plane wave excitation of the system shown in Figure 8, with the results obtained by the diakoptic method being compared with the reference WIPL-D solution. Excellent agreement of the two sets of results is observed from the figure. The total number of unknowns used for modeling in WIPL-D if no symmetries were exploited is 110,592. Similarly to the first example, when comparing the diakoptic approach to the pure MoM higher-order solution (WIPL-D), the reduction in the number of unknowns in the final system of equations is by two times. However, note that the higher-order FEM-MoM-diakoptic method would allow modeling of inhomogeneous and/or anisotropic scatterers in the array in Figure 8 at essentially the same computational cost. Running the FEM-MoM-diakoptic parallel code on a 16×16 -process grid, on 16 compute nodes (16 processes per node), the simulation time is 30 min 12 sec, and the RAM consumption for the storage of the diakoptic matrices is 91.1 GB. Note also that when compared to the higher-order diakoptic solution, the low-order diakoptic model specified in Section 3.1 would require 7.11 times more diakoptic unknowns, about 358 times longer direct-solver solution time and about 50 times larger RAM.

3.4. 2-D Array of PEC Spheres with Cloaking Dielectric/Magnetic Metamaterial Covers

The final example is a 2-D array of cloaked spherical PEC scatterers, depicted in Figure 10. The radii of the PEC spheres are $R_1 = 1$ m, thicknesses of the cloaks are $d = 0.1$ m (outer radii of the cloaks are $R_2 = R_1 + d$), and distances between the scatterer centers are $L = 5$ m. Each transformation-based metamaterial spherical cloak relies on the theory derived in Pendry et al. (2006), whereas its detailed analysis by the higher-order FEM-MoM can be found in Savić et al. (2013). The scatterer geometry and incident plane wave direction are shown in Figure 10. In the FEM-MoM-diakoptic analysis, each of the cloaked regions is modeled by six curvilinear hexahedra of fourth geometrical orders, $K_u = K_v = K_w = 4$, enclosed by six quadrilaterals conformal to the outer cloak surface. The adopted field approximation orders are $N_u = N_v = N_w = 5$ for all FEM hexahedra, while the current approximation orders are $N_u = N_v = 4$ for all MoM patches. The total number of diakoptic unknowns amounts to $D = 768$. Continuous

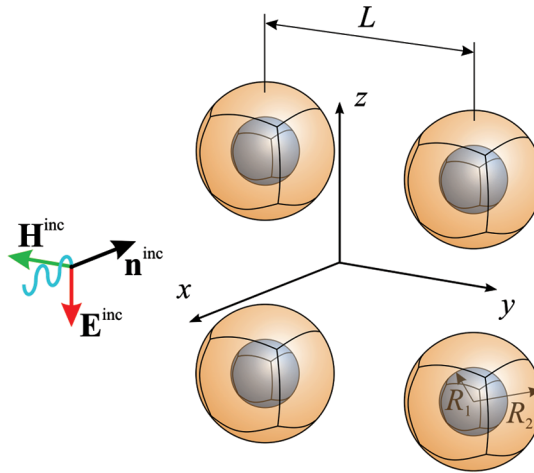


Figure 10. 2-D array of PEC spheres with cloaking metamaterial covers; permittivity and permeability tensors are given in Eq. (15).

spatial variations of the medium tensors $\overline{\overline{\epsilon}}$ and $\overline{\overline{\mu}}$ in the cloaked regions, obtained from the linear cloak transformation in the spherical (r, θ, ϕ) coordinate system, are given by (Savić et al., 2013)

$$\overline{\overline{\epsilon}} = \overline{\overline{\mu}} = \begin{bmatrix} \frac{R_2(R_1 - r)^2}{(R_2 - R_1)r^2} & 0 & 0 \\ 0 & \frac{R_2}{R_2 - R_1} & 0 \\ 0 & 0 & \frac{R_2}{R_2 - R_1} \end{bmatrix}, \quad (15)$$

where R_1 and R_2 are the inner and outer radii, respectively, of the spherical cloak. The Cartesian equivalents of $\overline{\overline{\epsilon}}$ and $\overline{\overline{\mu}}$ are implemented using Eq. (7) with $M_u = M_v = M_w = 6$.

Shown in Figure 11 is the normalized backscattering RCS of the array of cloaked spheres at $f = 55$ MHz obtained by the FEM-MoM-diakoptic method in the $\phi = 0$ plane. For the purpose of validation of the numerical solution, the computed RCS of the array of uncloaked PEC spheres, with the continuously inhomogeneous anisotropic FEM elements constituting the cloaking layer being replaced by homogeneous air-filled elements having all field and current expansions and other parameters in the FEM-MoM-diakoptic analysis the same as in the cloak model, is also shown in Figure 11, where it is compared with the WIPL-D solution, and excellent agreement of the two sets of results is observed. In addition, while having in mind that the cloak is theoretically ideal (RCS theoretically vanishes), a WIPL-D solution for a homogeneous air-filled sphere is shown as a reference, giving a clear insight into what a typical numerical solution for the given geometry and an ideal invisibility material (scattering from free-space) would be. A very significant reduction in the numerically obtained scattering cross-section of the array of cloaked spheres with respect to the array of PEC spheres is observed from the figure; namely, the RCS is so low that it is on par with the best numerical approximation of

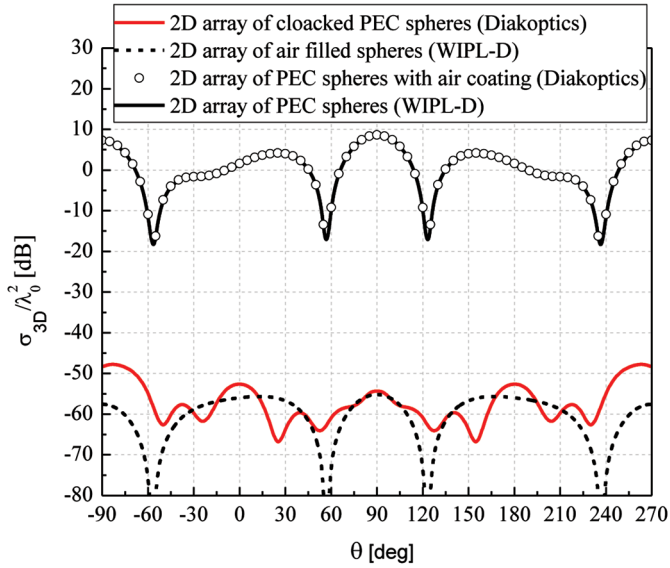


Figure 11. Normalized bistatic RCS in the $\phi = 0$ plane of: (i) the cloaked array in Figure 10 computed using FEM-MoM-diakoptics, (ii) the array of homogeneous air-filled spheres obtained using WIPL-D, (iii) the array of uncloaked spheres with cloaks replaced by homogeneous air layers calculated by FEM-MoM-diakoptics, and (iv) the array of PEC spheres obtained by WIPL-D.

the zero backscatter from an empty spherical region of the same size as the original scatterer, as verified by WIPL-D. The total number of FEM unknowns is $N_{\text{tot}}^e = 2,260$ (computation time: 24 min 5 sec, RAM: 18 MB, single process), while the total numbers of unknowns in WIPL-D simulations are 3,456 for the array of air-filled spheres and 1,728 for the array of PEC spheres.

4. Conclusions

This article has presented a new FEM-MoM-diakoptic method for analysis of inhomogeneous anisotropic dielectric and magnetic scatterers in the frequency domain. The method splits the original electromagnetic system into a number of closed-region FEM diakoptic subsystems containing material complexities and an open-region MoM diakoptic subsystem. Each of the subsystems is analyzed completely independently applying FEM or MoM solvers, and the solution to the original problem is obtained from linear relations between coefficients in expansions of equivalent electric and magnetic surface currents on diakoptic boundary surfaces. The method implements large curved hexahedral finite elements filled with inhomogeneous anisotropic materials. Diakoptic electric sources and the magnetic field in FEM subsystems are connected using dual sets of hierarchical polynomial vector basis functions explicitly satisfying the natural relation between curl-conforming and divergence-conforming quantities. A technique enabling touching of the subsystems, i.e., that the subsystems share a common diakoptic boundary, has been introduced in the diakoptic method.

The proposed higher-order FEM-MoM-diakoptic method and its versatility, accuracy, and efficiency have been validated and demonstrated in several characteristic examples

of finite arrays of dielectric, dielectric/magnetic, and dielectrically coated PEC scatterers. Numerical results include analysis of scatterers with straight edges and pronounced curvature, a scatterer modeled by multiple touching FEM diakoptic domains, and a transformation-based metamaterial cloaking structure, with the continuously inhomogeneous anisotropic cloaking region modeled using large curved finite elements that allow continuous spatial variations of complex permittivity and permeability tensors and high-order FEM field approximations.

Funding

This work was supported by the National Science Foundation (grants ECCS-1002385 and ECCS-1307863) and by the Serbian Ministry of Education, Science, and Technological Development (grant TR-32005).

References

- Cray Inc. 2011. *Cray XT6m*. Available online at <http://www.cray.com/>.
- Djordjević, M., & B. M. Notaroš. 2004. Double higher order method of moments for surface integral equation modeling of metallic and dielectric antennas and scatterers. *IEEE Trans. Ant. Propagat.* AP-52:2118–2129.
- Harrington, R. F. 2001. *Time-harmonic electromagnetic fields*, chap. 3, 106–110. New York: John Wiley & Sons.
- Ilić, M. M., & B. M. Notaroš. 2003. Higher order hierarchical curved hexahedral vector finite elements for electromagnetic modeling. *IEEE Trans. Microw. Theory Techn.* MTT-51:1026–1033.
- Ilić, M. M., & B. M. Notaroš. 2009. Higher order FEM-MoM domain decomposition for 3-D electromagnetic analysis. *IEEE Antennas Wireless Propag. Lett.* 8:970–973.
- Ilić, M. M., M. Djordjević, A. Ž. Ilić, & B. M. Notaroš. 2009. Higher order hybrid FEM-MoM technique for analysis of antennas and scatterers. *IEEE Trans. Ant. Propagat.* AP-57:1452–1460.
- Jin, J. M., & D. J. Riley. 2008. *Finite element analysis of antennas and arrays*, sect. 3.3, 77–86. New York: John Wiley & Sons.
- Kolundžija, B. M., & A. R. Djordjević. 2002. *Electromagnetic modeling of composite metallic and dielectric structures*, chap. 3, 116–119. Norwood, MA: Artech House.
- Kron, G. 1963. *Diakoptics: The piecewise solution of large scale systems*. London: MacDonald.
- Lee, S.-C., M. N. Vouvakis, & J.-F. Lee. 2005. A nonoverlapping domain decomposition method with nonmatching grids for modeling large finite antenna arrays. *J. Comput. Phys.* 203:1–21.
- Li, Y. J., & J. M. Jin. 2007. A new dual-primal domain decomposition approach for finite element simulation of 3-D large-scale electromagnetic problems. *IEEE Trans. Ant. Propagat.* AP-55: 2803–2810.
- Manić, A. B., S. B. Manić, M. M. Ilić, & B. M. Notaroš. 2012a. Large anisotropic inhomogeneous higher order hierarchical generalized hexahedral finite elements for 3-D electromagnetic modeling of scattering and waveguide structures. *Microw. Opt. Technol. Lett.* 54:1644–1649.
- Manić, A. B., D. I. Olčan, M. M. Ilić, & B. M. Notaroš. 2013. Diakoptic FEM-MoM analysis using explicit connection between field and current bases. *Proceedings of the 2013 IEEE Antennas and Propagation Society International Symposium*, Orlando, FL, 7–13 July.
- Manić, A. B., D. I. Olčan, M. M. Ilić, & B. M. Notaroš. 2012b. FEM-MoM-diakoptic analysis of scatterers with anisotropic inhomogeneities using hierarchical vector bases on large curved elements. *11th International Workshop on Finite Elements for Microwave Engineering (FEM2012)*, Estes Park, CO, 4–6 June.
- Notaroš, B. M. 2008. Higher order frequency-domain computational electromagnetics. *IEEE Trans. Ant. Propagat.* AP-56:2251–2276.

- Notaroš, B. M., & B. D. Popović. 1997. Optimized entire-domain moment-method analysis of 3D dielectric scatterers. *Int. J. Numer. Model.* 10:177–192.
- Olćan, D. I., M. M. Ilić, B. M. Notaroš, B. M. Kolundžija, & A. R. Djordjević. 2010. Diakoptic higher-order FEM-MoM approach. *Proceedings of the 2010 IEEE Antennas and Propagation Society International Symposium*, Toronto, Canada, 11–17 July.
- Olćan, D. I., I. M. Stevanović, B. M. Kolundžija, J. R. Mosig, & A. R. Djordjević. 2008a. Diakoptic surface integral-equation formulation applied to large antenna arrays. *Proceedings of the 2008 IEEE Antennas and Propagation Society International Symposium*, San Diego, CA, 5–12 July.
- Olćan, D. I., I. M. Stevanović, J. R. Mosig, & A. R. Djordjević. 2006. Diakoptic approach to analysis of microwave transmission lines. *Proceedings of the 36th European Microwave Conference*, Manchester UK, 10–15 September, 291–294.
- Olćan, D. I., I. M. Stevanović, J.R. Mosig, & A. R. Djordjević. 2007. Diakoptic surface integral-equation formulation applied to large 2-D scattering problems. *EuCAP*, Edinburgh, UK, 11–16 November.
- Olćan, D. I., I. M. Stevanović, J. R. Mosig, & A. R. Djordjević. 2008b. Diakoptic approach to analysis of multiconductor transmission lines. *Microw. Opt. Techn. Lett.* 50:931–936.
- Pendry, J. B., D. Schurig, & D. R. Smith. 2006. Controlling electromagnetic fields. *Science* 5781:1780–1782.
- Savić, S. V., A. B. Manić, M. M. Ilić, and B. M. Notaroš. 2013. Efficient higher order full-wave numerical analysis of 3-D cloaking structures. *Plasmonics* 8:455–463.
- WIPL-D d.o.o. 2013. *WIPL-D Pro v11.0*. Available online at <http://www.wipl-d.com/>.
- Zhao, K., V. Rawat, & J.-F. Lee. 2008. A domain decomposition method for electromagnetic radiation and scattering analysis of multi-target problems. *IEEE Trans. Ant. Propagat.* AP-56: 2211–2221.